

Study of the Reaction $\pi^+p \rightarrow \Sigma^+K^+$ between 1850- and 2090-MeV c.m. Energy*

G. E. KALMUS, G. BORREANI,† AND J. LOUIE‡

Lawrence Radiation Laboratory, University of California, Berkeley 94720

(Received 21 May 1970)

Angular distributions and polarization measurements (obtained from bubble-chamber data) are presented at seven incident π^+ momenta in the reaction $\pi^+p \rightarrow \Sigma^+K^+$. Results of a partial-wave analysis as well as an s -, t -, and u -channel analysis are presented. The branching fraction of the $\Delta(1950) \rightarrow \Sigma^+K^+$ was found to be $(2.0 \pm 0.4)\%$.

I. INTRODUCTION

THE aim of the experiment was to determine the branching fraction of the $\Delta(1950) \rightarrow \Sigma^+K^+$. To achieve this, we report on data taken at seven incident π^+ momenta between 1.34 and 1.84 GeV/c, using the 72- and 25-in. hydrogen bubble chambers at Lawrence Radiation Laboratory, Berkeley. The data have been analyzed by use of two approaches: (i) an s -channel partial-wave analysis, and (ii) an analysis using resonances in the s channel and exchanges in the t and u channels to account for the nonresonant "background" amplitudes. This second method is similar to that used by Evans and Knight¹ and by Holladay.²

Preliminary data on three of these energies were presented at Vienna.³

II. EXPERIMENTAL DETAILS

A. Exposure

Table I summarizes the data taken. This doubles the world's data in this energy region; the largest previous sample is from the experiment by Pan and Forman at a single momentum (1.7 GeV/c).⁴

TABLE I. Summary of film used in this experiment.

π^+ momentum (GeV/c)	Number of pictures (1000)	μb equivalent* (approx)
1.34	52 ^b	0.4
1.43	41 ^b	0.5
1.55	121 ^c	0.8
1.63	164 ^c	0.5
1.68	47 ^b	0.5
1.77	122 ^c	0.7
1.84	119 ^c	0.9

* Cross section for one event.
^b 72-in. chamber.
^c 25-in. chamber.

* Work done under the auspices of the U. S. Atomic Energy Commission.

† Present address: Istituto di Fisica dell'Universita, Torino, Italy.

‡ Present address: Brookhaven National Laboratory, Upton, N. Y. 11973.

¹ L. E. Evans and J. M. Knight, Phys. Rev. **137**, B1232 (1965).

² W. G. Holladay, Phys. Rev. **139**, B1348 (1965).

³ G. Borreani and G. E. Kalmus (unpublished).

⁴ Y. L. Pan and F. L. Forman, Nucl. Phys. **B16**, 61 (1970).

B. Scanning and Measuring

The entire film was scanned twice for two-prong events in which one or both of the prongs had a kink, but in which no recoil at the kink was visible. The combined scanning efficiency was found to be 99% for events that were eventually accepted as

$$\pi^+p \rightarrow \Sigma^+K^+ \rightarrow \pi^+n.$$

The events were measured by using the COBWEB on-line Franckenstein system⁵ and put through the FOG-CLOUDY-FAIR system for reconstruction, constraining, and plotting. Events that either failed the geometry program or did not satisfy (with a reasonable χ^2) any of the hypotheses

$$\begin{aligned} \pi^+p &\rightarrow \Sigma^+K^+ \quad \text{with } \Sigma^+ \rightarrow p\pi^0 \text{ or } \pi^+n \\ &\rightarrow \Sigma^+K^+\pi^0 \\ &\rightarrow \Sigma^+\pi^+K^0 \end{aligned}$$

were remeasured, and then measured a third time if they failed again. Events that still failed were then examined by a physicist. It was found that most of these events were two-prongs (π^+p , $\pi^+p\pi^0$, or $\pi^+\pi^+n$), where one of the prongs scattered slightly but left no visible recoil. Others could have been $\Sigma^+K^+(\pi^0)$ or $\Sigma^+\pi^+(K^0)$, but the decay angle of the $\Sigma^+ \rightarrow \pi^+n$ was so small as to be impossible to measure in all views. These events were in any case rejected by our acceptance criteria (see Sec. III). It was found that about another 4% of these events appeared to be genuine on the scan table, were within the acceptance criteria, but had no acceptable output. The reason for this was usually obvious, such as one of the origins being obscured by other tracks in one of the views. This loss was taken into account in computing the cross sections.

The events were constrained in the following way.

(a) If $\Delta p/p$ (measured) for the Σ^+ was <0.5 , then a standard two-vertex fit was performed for both $\Sigma^+ \rightarrow p\pi^0$ and $\Sigma^+ \rightarrow \pi^+n$ hypotheses.

(b) If $\Delta p/p$ for the Σ^+ was >0.5 , the measured momentum of the Σ^+ was ignored and it was calculated from the decay vertex. This in general gave two values

⁵ H. C. Albrecht, E. P. Binnall, R. W. Birge, M. H. Myers, and P. W. Weber, Lawrence Radiation Laboratory Report No. UCRL-18528 Rev., 1968 (unpublished).

TABLE II. Summary of data and cross sections for $\pi^+p \rightarrow \Sigma^+K^+$.

Momentum of π^+ (GeV/c)	Energy, c.m. (GeV/c)	Number of events			Cross section $\pi^+p \rightarrow \Sigma^+K^+$ (μb)
		$\Sigma^+ \rightarrow p\pi^0$ (unweighted)	$\Sigma^+ \rightarrow \pi^+n$ (unweighted)	$\Sigma^+ \rightarrow \pi^+n$ (weighted)	
1.34	1.851	249	290	367	400 \pm 35
1.43	1.896	222	293	374	510 \pm 40
1.55	1.955	142	219	279	530 \pm 50
1.63	1.992	255	299	375	470 \pm 40
1.68	2.016	197	299	377	505 \pm 40
1.77	2.057	129	209	265	415 \pm 50
1.84	2.089	102	158	201	405 \pm 50

for each hypothesis ($p\pi^0$, π^+n), since it is a zero-constraint fit. These values were then used as starting values in the two-vertex simultaneous fit.

Ionization was used to resolve the $\Sigma^+ \rightarrow p\pi^0$ or $\Sigma^+ \rightarrow \pi^+n$ ambiguity.

In order to obtain cross sections, the beam tracks were counted on about every hundredth frame in the film, and from this the total π^+ path length in the experiment was computed.

III. DATA

Table II shows the number of events found at each energy that satisfies the following cuts.

(a) The beam track is within the acceptable angular and momentum limits.

(b) Σ^+ is >0.3 cm long and lives less than three lifetimes.

(c) The Σ^+ decay angle (lab) is $>5^\circ$ ($>10^\circ$ for 72-in. chamber film).

(d) The event is within the fiducial volume.

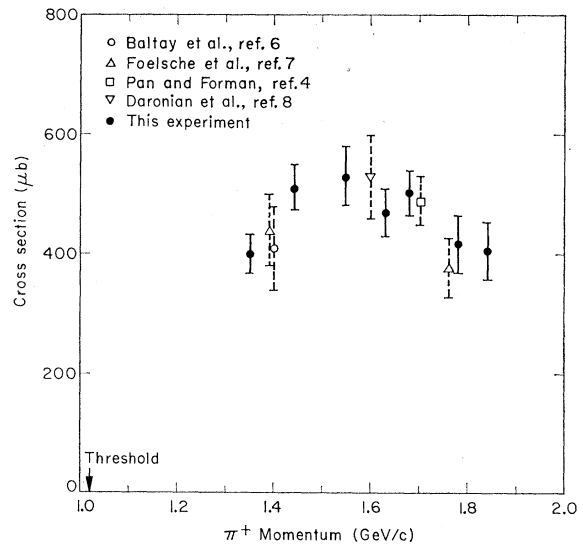
Since cuts (b) and (c) are Σ^+ -momentum-dependent, each event was weighted to take into account these two cuts as well as the possibility that the Σ^+ left the chamber before decaying. The values of cuts (b) and (c) were determined experimentally. For (b) we used the Bartlett s -function method to determine the Σ lifetime. The lifetime was calculated as a function of Σ^+ cutoff length and was found to become stable at a length of 0.3 cm. Cut (c) was determined using the following iterative procedure. From the measured Σ^+ momentum spectrum, we generated by Monte Carlo methods the expected Σ^+ decay angular distribution in the laboratory and compared it to the measured one. From this we determined a first approximation to the cut. We then corrected accordingly the Σ^+ momentum spectrum and repeated the procedure. Convergence was essentially obtained in a single step for the $\Sigma^+ \rightarrow \pi^+n$ mode. It should be noted that these cuts are critical only for the $\Sigma^+ \rightarrow \pi^+n$ decay mode, since the angular distributions and cross sections have been determined by use of this mode only. For the polarization measurement using the $\Sigma^+ \rightarrow p\pi^0$ mode, unweighted events were used, since the polarization measurement is not affected by any bias in the decay angular distribution.

A. Cross Sections

Figure 1 and Table II show the cross sections for $\pi^+p \rightarrow \Sigma^+K^+$.⁶⁻⁸ These were obtained by using the weighted number of $\Sigma^+ \rightarrow \pi^+n$ events and multiplying by 2.12 to take into account the $\Sigma^+ \rightarrow p\pi^0$ decay mode.⁹ The error bars shown contain both statistical and systematic effects. The other data points on the plot have been obtained from the literature.

B. Angular Distributions

The angular distributions at the seven momenta for both the weighted and unweighted $\pi^+p \rightarrow \Sigma^+K^+$, $\Sigma^+ \rightarrow \pi^+n$ events are shown in Fig. 2. The production cosine, $\cos\theta$, used is the cosine of the angle (c.m.) between the incident π^+ and outgoing K^+ , i.e., $(\hat{\pi}^+ \cdot \hat{K}^+)$ (c.m.). The average weight per event is about 1.25, and

FIG. 1. Cross section for $\pi^+p \rightarrow \Sigma^+K^+$.

⁶ C. Baltay, H. Courant, W. J. Fickinger, E. C. Fowler, H. L. Kraybill, J. Sandweiss, J. R. Sanford, D. V. Stonehill, and H. Taft, *Rev. Mod. Phys.* **33**, 374 (1961).

⁷ H. W. J. Foelsche, A. Lopez-Cepero, C. Y. Chien, and H. L. Kraybill (unpublished).

⁸ P. Daronian, A. Daudin, M. A. Jabiol, C. Lewin, C. Kochowski, B. Ghidini, S. Mongelli, and V. Picciarelli, *Nuovo Cimento* **41**, 771 (1966).

⁹ Particle Data Group, *Rev. Mod. Phys.* **41**, 109 (1969).

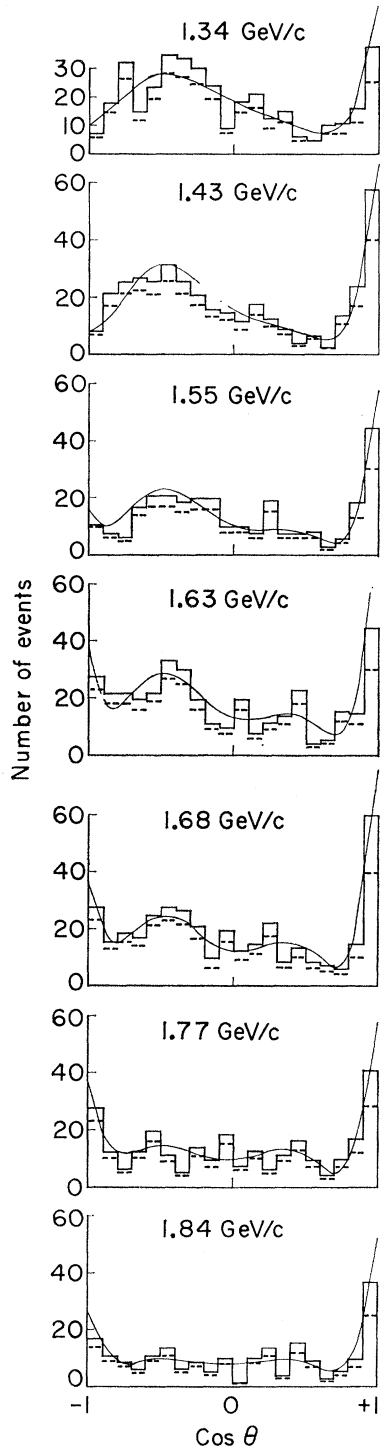


FIG. 2. Angular distributions at the seven momenta for $\pi^+p \rightarrow \Sigma^+K^+$, $\Sigma^+ \rightarrow \pi^+n$. The solid boxes are the weighted events; the dashed boxes are the unweighted events. The curve is from fit 192A [see Table III and Fig. 7(b)]; $\cos\theta$ is defined as $(\hat{p}^+ \cdot \hat{K}^+)$ (c.m.).

it is not greater than 1.6 for any bin. We decided not to use the $\Sigma^+ \rightarrow p\pi^0$ events, since the average weight for these was about 2, and was greater for some of the bins.

There is also evidence that the scanning efficiency for these events was lower than for $\Sigma^+ \rightarrow \pi^+n$ events, with the proton being in the plane containing the camera optic axis and the direction of the Σ^+ . The same bias was not present in the $\Sigma^+ \rightarrow \pi^+n$ events.

C. Polarizations

Since the Σ^+ decay is parity violating, the angular distribution of the decay particles in the Σ^+ rest frame must be of the form

$$d\sigma/d(\cos\theta_N) = 1 + \alpha \bar{P}_\Sigma \cos\theta_N,$$

where α is the asymmetry parameter, \bar{P}_Σ is the average polarization of the Σ , and $\cos\theta_N$ is defined as $(\hat{n} \cdot \hat{N})$, where \hat{n} is the production normal [$\hat{n} = (\hat{p}^+ \times \hat{K}^+)/|\hat{p}^+ \times \hat{K}^+|$], and \hat{N} is a unit vector parallel to the nucleon direction from the Σ^+ decay.

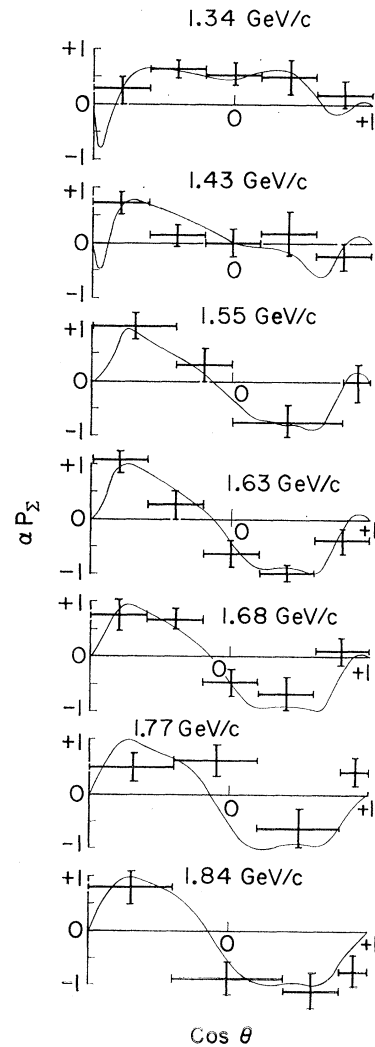


FIG. 3. Plot of $\alpha \bar{P}_\Sigma$ versus $\cos\theta$, at the seven momenta for $\Sigma^+ \rightarrow p\pi^0$ events ($\alpha \approx -1$). The curve is from fit 192A [see Table III and Fig. 7(b)].

Figures 3 and 4 show $\alpha\bar{P}_\Sigma$ as a function of the c.m. production angle; the events at each energy were divided into bins in $\cos\theta$ having ≈ 30 events per bin. For each bin the Σ polarization was calculated from the observed Σ -decay asymmetry relative to the production normal \hat{n} , according to the formula

$$\alpha\bar{P} = \frac{3}{N_E} \sum_{i=1}^{N_E} \cos\theta_{N_i}$$

and

$$\Delta(\alpha\bar{P}) = \left[\frac{3 - (\alpha\bar{P})^2}{N_E} \right]^{1/2}$$

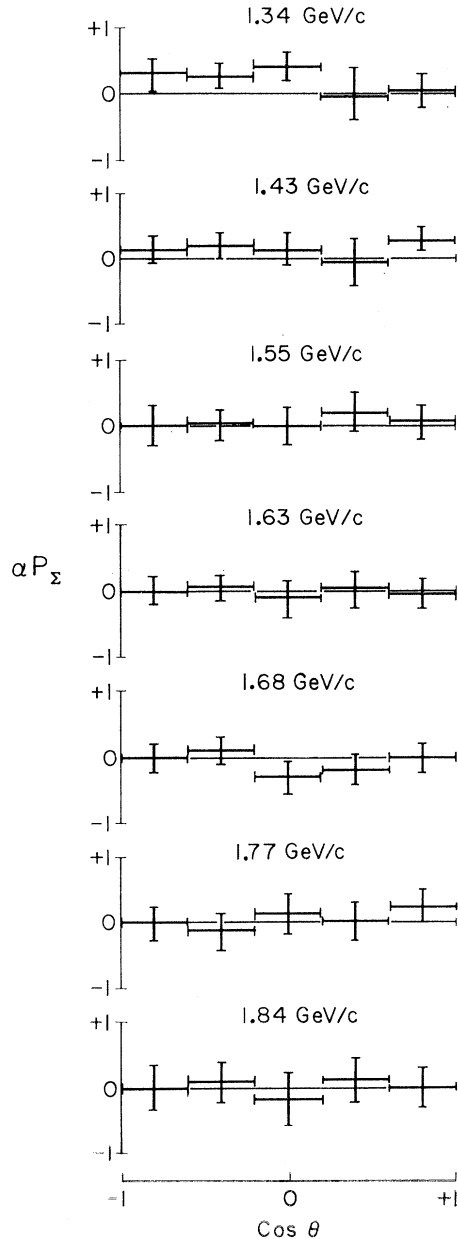


FIG. 4. Plot of $\alpha\bar{P}_\Sigma$ versus $\cos\theta$, at the seven momenta, for $\Sigma^+ \rightarrow \pi^+ n$ events ($\alpha \approx 0$).

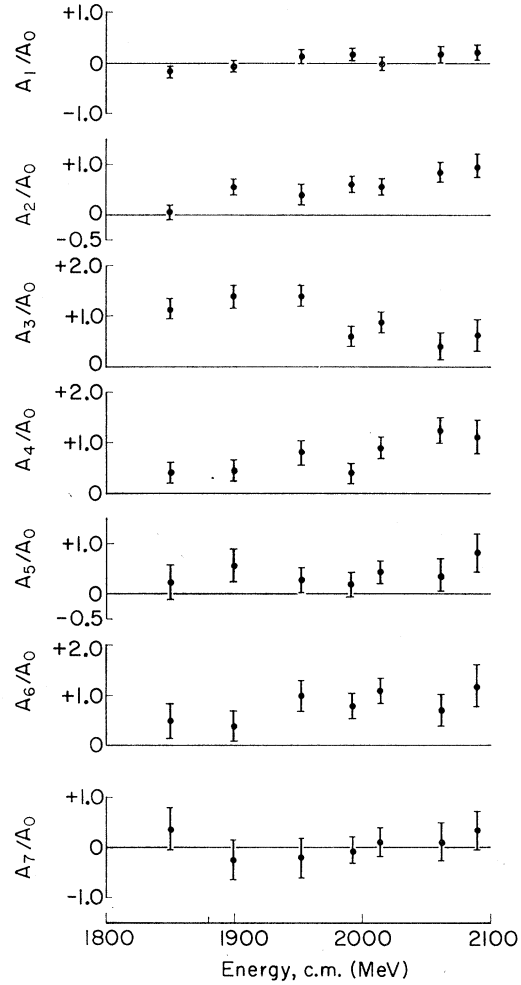


FIG. 5. Plots of A_1/A_0 - A_7/A_0 at each of the seven momenta. The A 's were calculated by fitting the weighted angular distributions (Fig. 2) with the Legendre series (see Sec. IV) up to the seventh order. The sixth order was the maximum necessary to obtain a good fit at all momenta.

(when $|\alpha\bar{P}|$ was > 1 , $|\alpha\bar{P}| = 1$ was used in the error formula). N_E is the number of events in each bin.

The maximum-likelihood method was also used to obtain $\alpha\bar{P}$, and the two methods were found to be in excellent agreement.

D. Legendre Expansions

Figure 5 shows the values of A_m/A_0 of the Legendre polynomials fitted to the distributions shown in Fig. 2, where the expression

$$\frac{d\sigma}{d\Omega} = \lambda^2 \sum_{m=0}^{m_{\max}} A_m P_m(\cos\theta)$$

has been used. Figure 6 shows the values of the expansion coefficients B_n/A_0 of the first associated Legendre series when fitted to the polarization distributions

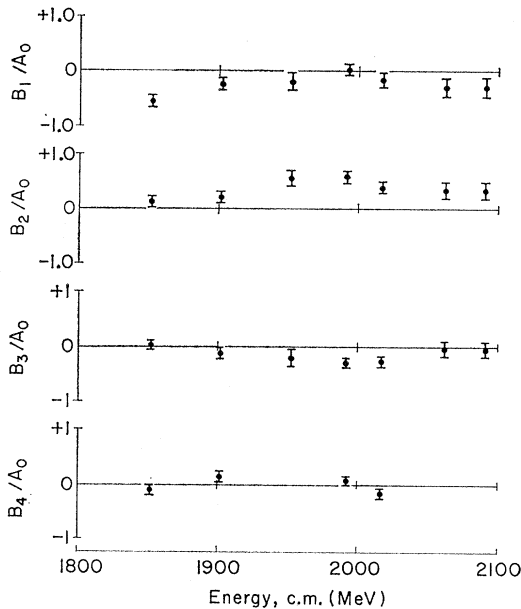


FIG. 6. Plots of B_n/A_0 at each of the seven momenta. These were calculated by fitting the αP_2 plots ($\Sigma^+ \rightarrow p\pi^0$) (Fig. 3) with the first associated Legendre series (see Sec. IV) up to the maximum order allowed by the number of boxes in the data ($m = \text{number of boxes} - 1$). It should be noted that in most cases this order was *not* sufficient to give a good fit.

shown in Fig. 3, where the expression

$$\frac{d\sigma}{d\Omega} \mathbf{P} = \hat{n} \lambda^2 \sum_{n=1}^{n_{\max}} B_n P_n^1(\cos\theta)$$

was used.

For the A_n/A_0 distributions, the coefficients from the seventh-order fit were plotted. At all momenta the sixth-order fit was found to be satisfactory. For the B_n/A_0 distributions the maximum order allowed by the number of experimental bins was plotted (where we define the maximum order to be the number of bins minus one)—this did not give a satisfactory fit at most momenta. It should be noted that the fits of the models to the data do not depend on a knowledge of the A and B coefficients (see Sec. V).

IV. THEORY

When one examines the cross sections and angular distributions (Figs. 1 and 2) of $\pi^+p \rightarrow \Sigma^+K^+$, it is clear that in this energy region s -channel effects are large and, in particular, the bump in the cross section at a mass of ≈ 1950 MeV is very suggestive of an s -channel resonance. We have therefore used two approaches to the analysis of the data: (a) an s -channel energy-dependent partial-wave analysis, in which both resonant and nonresonant amplitudes are present, and (b) an s -, t -, and u -channel analysis in which we have resonances in the s channel and K^* and Λ exchange in the t and u channels to account for the background

amplitudes. We are aware of the dangers of double counting in this latter approach, but believe the results show that this is not serious in this case.

A. Partial-Wave Analysis

A comprehensive discussion of the theory of partial-wave analysis in formation experiments can be found in Tripp,¹⁰ so only a brief discussion is given here.

In a reaction of spin $0 + \text{spin } \frac{1}{2} \rightarrow \text{spin } 0 + \text{spin } \frac{1}{2}$ the transition operator M is given by

$$M = a(\theta) + b(\theta) \boldsymbol{\sigma} \cdot \hat{n}. \quad (1)$$

In this formula, a and b are the non-spin-flip and the spin-flip amplitudes, respectively. The production angle θ and production normal \hat{n} have been defined earlier (Secs. III B and III C) and $\boldsymbol{\sigma}$ is the Pauli spin operator. The relationships between $a(\theta)$ and $b(\theta)$ and the complex partial-wave amplitudes T_l^\pm (l is the final orbital angular momentum) are

$$a(\theta) = \lambda \sum_l [(l+1)T_l^+ + lT_l^-] P_l(\cos\theta),$$

$$b(\theta) = i\lambda \sum_l (T_l^+ - T_l^-) P_l^1(\cos\theta), \quad (2)$$

where λ is the π^+ wavelength in the c.m. system divided by 2π , superscripts \pm refer to $J = l \pm \frac{1}{2}$, P_l is the l th-order Legendre polynomial, and P_l^1 is the l th-order first associated Legendre polynomial.

The differential cross section I and polarization \mathbf{P} are given by

$$I (= d\sigma/d\Omega) = |a|^2 + |b|^2$$

$$\text{and} \quad I\mathbf{P} = 2 \text{Re}(a^*b)\hat{n}, \quad (3)$$

where the polarization is limited to being along the production normal by parity conservation of the strong interaction.

A more direct relationship between the measured distributions I and $I\mathbf{P}$ and the partial-wave amplitudes is obtained by making the expansions

$$I = \lambda^2 \sum_{m=0} A_m P_m(\cos\theta)$$

and

$$I\mathbf{P} = \hat{n} \lambda^2 \sum_{n=1} B_n P_n^1(\cos\theta).$$

The relationship between the A and B coefficients and the partial-wave amplitudes T^\pm is well known, and is given (for example) in Ref. 10.

The amplitudes T^\pm (and A_m and B_n) are, in general, functions of the c.m. energy. The variation of T^\pm with energy is in most cases unknown; the exception is for a resonant amplitude when this energy dependence is assumed to be given by the Breit-Wigner formula

$$T = \frac{1}{2} (\Gamma_e \Gamma_r)^{1/2} / [(E_R - E) - i\Gamma/2],$$

¹⁰ R. D. Tripp, in *International School of Physics "Enrico Fermi"* (Academic, New York, 1966), Course 33, p. 70.

where E is the c.m. energy, E_R is the energy of the resonance, Γ_e is the partial width into the elastic channel, Γ_r is the width into the final (reaction) channel, and Γ is the total width $= \sum_i \Gamma_i$, where i are all the decay channels.

The partial widths Γ_i are also, in general, energy dependent. This energy dependence has been approximated by Glashow and Rosenfeld¹¹ by

$$\Gamma_i \propto \left(\frac{q_i^2}{q_i^2 + X^2} \right)^{l_i} \frac{q_i}{E},$$

where q_i and l_i are the momentum and orbital angular momentum of the decay products of the resonance into the i th channel, and X is a parameter related to the radius of the interactions and has the dimensions of mass. Blatt and Weisskopf have also derived non-relativistically an expression for the energy dependence of Γ_i , which is identical to the above for $l \leq 1$ and differs only slightly for higher values of l .¹²

The problem is to solve Eqs. (2) and (3) for the T_{fi}^\pm given the experimental distributions I and IP . This requires nonlinear least-squares minimization, and we use the computer program VWAVE to solve it.¹³

In this program the inputs are the I and IP distributions and the total channel cross section at each energy. A set of starting values for each amplitude T_{fi}^\pm is then chosen. These could be either of the resonant form with an energy-dependent width, or background amplitudes with an energy dependence of the form $(A+Bk)e^{i(C+Dk)}$, where k is the incident c.m. momentum. There were, therefore, four parameters for each partial wave (or eight if a resonant and a background amplitude were postulated for any partial wave). For the background amplitudes these are clearly A , B , C , and D ; for a resonance these are magnitude $|\Gamma_e \Gamma_r|^{1/2}$, mass E_R , half-width $\frac{1}{2}\Gamma$, and phase ϕ (at resonance).

The starting values were used to calculate the cross sections, angular distributions, and polarizations. The calculated quantities X_i^e were compared with the observed data X_i^0 and their errors ΔX_i^0 to find the χ^2 :

$$\chi^2 = \sum_i [(X_i^e - X_i^0) / \Delta X_i^0]^2,$$

where i runs over all the experimental points.

The χ^2 function was then minimized with respect to all the parameters by the variable metric method by using the Lawrence Radiation Laboratory program VARMIT.¹⁴ After a satisfactory minimum is obtained, the values of the parameters are randomly displaced from their minimum values and the minimization is

¹¹ S. L. Glashow and A. H. Rosenfeld, Phys. Rev. Letters **10**, 192 (1963).

¹² J. M. Blatt and V. F. Weisskopf, *Theoretical Nuclear Physics* (Wiley, New York, 1966), p. 389.

¹³ W. M. Smart, thesis, Lawrence Radiation Laboratory Report No. UCRL-17712, 1967 (unpublished).

¹⁴ E. R. Beals, Program VARMIT Write-Up, Lawrence Radiation Laboratory Computer Library Note (unpublished).

repeated. This was repeated twice, and the lowest χ^2 solution was printed out. This method helps to ensure that the program does not stop at a shallow local minimum.

In our search for minima we have started at more than 200 sets of initial conditions. We have also used the program MINFUN¹⁵ in its search mode, which explores the valleys in the χ^2 hypersurface, to try to establish the uniqueness of the best solution found. It should be noted that the confidence in the results of the fit depends to a certain extent on whether the parametrization of the background amplitudes is realistic.

B. s-, t-, and u-Channel Analysis

This analysis assumes s-channel resonances and t- and u-channel exchanges comprising the nonresonant "backgrounds." As noted earlier, similar approaches have been made,^{1,2} but to establish conventions we will write the relevant equations in some detail.

In terms of the Dirac matrices γ_μ and spinors u_p and u_Σ , the Feynman amplitude for the reaction $\pi^+ p \rightarrow \Sigma^+ K^+$ may be written, in general,¹⁶

$$F_{fi} = \bar{u}_\Sigma(p') [A + \frac{1}{2} B \gamma_\mu (k + k')_\mu] u_p(p),$$

where k , k' , p , and p' are the four-momenta of the π , K , p , and Σ , respectively, and A and B are functions of the total c.m. energy E and the cosine of the c.m. production angle θ as defined earlier.

The production amplitude is related to F_{fi} by

$$T_{fi} = \frac{(mm')^{1/2}}{4\pi} \frac{1}{E} \left(\frac{|\mathbf{k}'|}{|\mathbf{k}|} \right)^{1/2} F_{fi},$$

where m is the proton mass and m' is the Σ mass. In terms of Pauli spinors and matrices, $T_{fi} = \chi_f^\dagger M \chi_i$, where the transition operator is

$$M = g + h(\boldsymbol{\sigma} \cdot \hat{p}')(\boldsymbol{\sigma} \cdot \hat{p}).$$

The amplitudes g and h are related to A and B by

$$g = C_+ [A + \frac{1}{2} B(2E - m - m')]$$

and

$$h = C_- [-A + \frac{1}{2} B(2E + m + m')],$$

where

$$C_\pm = \left(\frac{|\mathbf{k}'|}{|\mathbf{k}|} \right)^{1/2} \frac{1}{8\pi E} [(p_0 \pm m)(p_0' \pm m')]^{1/2}.$$

Here p_0 is the c.m. energy of the proton, p_0' of the Σ . In terms of the more familiar non-spin-flip and spin-flip amplitudes a and b , the transition operator M may be expressed as in Eq. (1), where a and b are related to g and h by $a = g + h \cos\theta$ and $b = -ih \sin\theta$. The differential cross section and Σ polarization are now given as before [Eq. (3)].

¹⁵ W. E. Humphrey, Program MINFUN Write-Up, Lawrence Radiation Laboratory Computer Library Note (unpublished).

¹⁶ G. F. Chew, M. L. Goldberger, F. E. Low, and Y. Nambu, Phys. Rev. **106**, 1337 (1957).

1. Resonant Terms

The s -channel resonant contributions a_s and b_s to the amplitudes a and b have the same expansions as Eq. (2), where the partial-wave amplitudes T_l are approximated by the Breit-Wigner form and the partial widths are also parametrized as before. For each resonant partial wave, four variable parameters are possible, as in the s -channel analysis: magnitude $|\Gamma_e \Gamma_r|^{1/2}$, mass E_R , and width $\frac{1}{2}\Gamma$, and a relative phase ϕ .

2. Exchange Terms

We assume that the exchange contributions to a and b come from terms representing K^* exchange in the t channel and Λ exchange in the u channel.

t channel. For the exchange of a vector meson K^* with mass M and unit polarization vector e_μ , the invariant amplitude may be constructed¹⁷ from the meson vertex factor

$$\sqrt{2}g_{K^*K\pi}(k+k')_\mu e_\mu,$$

the baryon vertex factor

$$\sqrt{2}\bar{u}_\Sigma(p')\left(G_V\gamma_\nu+iG_T\frac{\sigma_{\nu\lambda}q_\lambda}{m+m'}\right)u_p(p)e'_\nu,$$

and the vector-meson propagator

$$(-g_{\mu\nu}+q_\mu q_\nu/M^2)/(q^2-M^2).$$

The constant $\sqrt{2}$ is an isospin factor, $g_{K^*K\pi}$ is the coupling constant at the meson vertex, and G_V is the vector (and G_T the tensor) coupling constant at the baryon vertex. The metric is $g_{\mu\mu}=(1, -1, -1, -1)$, and q_μ is the four-momentum transferred between the initial and final mesons. By comparing the amplitude thus constructed and the general Feynman amplitude, one finds the identities

$$A_t = \frac{2}{2kk'(z_t - \cos\theta)} \left[\frac{(\mu'^2 - \mu^2)(m' - m)}{M^2} g_{K^*K\pi} G_V + \frac{2E^2 - m^2 - m'^2 - 2k_0 k'_0 + 2kk' \cos\theta}{m + m'} g_{K^*K\pi} G_T \right]$$

and

$$\frac{1}{2}B_t = \frac{2}{2kk'(z_t - \cos\theta)} (g_{K^*K\pi} G_V - g_{K^*K\pi} G_T),$$

where k and k' are now the magnitudes of the momenta of the initial and final mesons, k_0 and k'_0 are their c.m. energies, and μ and μ' are their masses. The kinematical factor is

$$z_t = (M^2 + 2k_0 k'_0 - \mu^2 - \mu'^2)/2kk',$$

and is approximately equal to 2 for the energies in this experiment. Once A_t and B_t are known, g_t and h_t —

¹⁷ J. D. Bjorken and S. D. Drell, *Relativistic Quantum Mechanics* (McGraw-Hill, New York, 1964).

and therefore a_t and b_t —may be calculated from

$$a_t = g_t + h_t \cos\theta$$

and

$$b_t = -ih_t \sin\theta.$$

(These purely Born exchange terms are real.) Multiplying these by a phase factor $e^{i\phi_t}$ yields complex amplitudes, in general, which express the relative phase between the s and t channels. The parameters for the t -channel exchange that can be varied are the coupling-constant products $g_{K^*K\pi}G_V$ and $g_{K^*K\pi}G_T$, and the arbitrary phase ϕ_t .

u channel. For the exchange of a Λ of mass M' , the invariant amplitude has the form

$$F = \bar{u}_\Sigma(p') \left(g_{\pi\Lambda\Sigma} \gamma_5 \frac{1}{\gamma_\mu q'_\mu - M'^2} \gamma_5 g_{N\Lambda K} \right) u_p(p),$$

where q'_μ is the four-momentum transferred between the initial π and final Σ . Reducing and comparing this expression with the general Feynman amplitude as before, one finds

$$A_u = - \frac{g_{\pi\Lambda\Sigma} g_{N\Lambda K}}{2kk'(z_u + \cos\theta)} \frac{1}{2} (2M' - m' - m)$$

and

$$\frac{1}{2}B_u = - \frac{1}{2} \frac{g_{\pi\Lambda\Sigma} g_{N\Lambda K}}{2kk'(z_u + \cos\theta)},$$

with the kinematical factor

$$z_u = (M'^2 + 2k_0 p'_0 - m'^2 - \mu^2)/2kk'$$

also approximately equal to 2. As in the t -channel exchange, a_u and b_u may now be calculated. The parameters that may be varied are the coupling constant product $g_{\pi\Lambda\Sigma} g_{N\Lambda K}$ and an arbitrary phase ϕ_u .

Form factors. The coupling "constant" products in the exchange channels are, in general, dependent on the square of the momentum transfer, and we have allowed for this possibility by applying multiplicative factors of the simple form¹⁸: For the t channel,

$$\frac{\alpha - M^2}{\alpha - t} = \frac{(\alpha - M^2)/2kk'}{z_t' - \cos\theta},$$

and for the u channel,

$$\frac{\beta - M'^2}{\beta - \mu} = \frac{(\beta - M'^2)/2kk'}{z_u' + \cos\theta},$$

where α and β are additional parameters which can be varied, and

$$z_t' = (\alpha + 2k_0 k'_0 - \mu^2 - \mu'^2)/2kk'$$

and

$$z_u' = (\beta + 2k_0 p'_0 - m'^2 - \mu^2)/2kk'.$$

¹⁸ G. Goldhaber, W. Chinowsky, S. Goldhaber, W. Lee, and T. O'Halloran, *Phys. Letters* 6, 62 (1963).

The effect of these form factors is to produce more peaking in the forward and backward directions in the angular distributions, and therefore to increase the relative importance of the higher partial waves in the exchange amplitudes.

Projection of exchange amplitudes. To compare in the complex T plane the s -channel resonant partial waves with the partial waves due to the exchange amplitudes, the latter, a_{exch} and b_{exch} , where $a_{\text{exch}} = a_t + a_u$ and $b_{\text{exch}} = b_t + b_u$, are first expanded in Eq. (2). The exchange partial-wave amplitudes T_l are then projected out into the s channel by means of relations such as

$$Q_l(z) = \frac{1}{2} \int_{-1}^1 \frac{P_l(\cos\theta)}{z - \cos\theta} d \cos\theta$$

and

$$Q_l^1(z) = -\frac{1}{2} \frac{1}{(z^2 - 1)^{1/2}} \int_{-1}^1 \frac{\sin\theta}{z - \cos\theta} P_l^1(\cos\theta) d \cos\theta,$$

where $Q_l(z)$ is the l th-degree Legendre polynomial of the second kind and $Q_l^1(z)$ is the first associated Legendre function of the second kind.

Once $a = a_s + a_t + a_u$ and $b = b_s + b_t + b_u$ are known, the differential cross sections and Σ polarizations may be calculated. The mechanics of the s -, t -, and u -channel analysis are identical to that described in Sec. IV A; inputs are the angular and Σ polarization distributions and total ΣK cross sections at each energy, as well as a set of starting values for the resonance parameters and exchange parameters. A χ^2 was formed from the calculated and observed distributions and cross sections, and minimized with respect to all the parameters allowed to vary. The number of variable parameters was usually four for each resonant amplitude plus up to a total of seven for the exchange amplitudes.

The exchange amplitudes were then projected into the s channel to be compared directly with the resonant-amplitude partial waves. The dominant partial waves from the exchange amplitudes were $S1$, $P1$, $P3$, and $D3$. Higher partial waves were in all cases very small.

V. AMBIGUITIES

A study of Eqs. (2) and (3) shows that there are several transformations that leave either I or IP or both unchanged. These are as follows.

(i) $T_l'^{\pm} = e^{i\phi} T_l^{\pm}$, where $T_l'^{\pm}$ are the transformed amplitudes; both I and IP are unchanged. This just states that the absolute phase of the amplitudes is arbitrary. It is usual to fix the phase of one amplitude, e.g., the phase of a resonance at its resonant energy is usually put to zero.

(ii) $T_l'^{\pm} = T_l^{\pm*}$. This is the complex conjugation ambiguity, and I remains unchanged but P changes sign.

(iii) $T_l'^{\pm} = T_{l-1}^{\mp}$ and $T_l'^{-} = T_{l-1}^{+}$, i.e., changing the parity of all amplitudes. This is the Minami ambiguity.

I remains unchanged and P changes sign. The ambiguity, keeps J fixed but changes l , e.g., $P3 \rightarrow D3$.

$$\begin{aligned} \text{(iv)} \quad T_l'^+ &= \pm (2l+1)^{-1} (T_l^+ + 2l T_l^-), \\ T_l'^- &= \pm (2l+1)^{-1} [2(l+1) T_l^+ - T_l^-]. \end{aligned}$$

This is the Yang transformation and leaves I unchanged but changes the sign of P . This transformation does not necessarily conserve unitarity, but for channels with low branching fractions this is not likely to be a problem. This transformation keeps l fixed and changes J ; e.g., $P3$ becomes a mixture of $P3$ and $P1$.

It should be noted that the application of transformations (ii) and (iii), (ii) and (iv), or (iii) and (iv) would result in both I and IP remaining unchanged. Thus, solutions related by either the generalized Minami ambiguity or generalized Yang transformation are indistinguishable in a study of the angular distributions and polarization. If, however, there is a known energy dependence of one of the amplitudes present, such as a resonance in which the Wigner condition specifies the direction in which the amplitude traverses the Argand diagram, both the generalized Minami and the Yang transformations reverse this direction and would therefore violate the Wigner condition. Performing both the Minami and the Yang transformations results in a set of amplitudes that gives the same angular distributions and polarizations and does not violate the Wigner condition. It does, however, have the effect of making two resonant amplitudes (the same mass and width) out of one.

VI. RESULTS

A. s -Channel Analysis

The data were split up into 100 bins in the angular distributions and 32 bins in the polarization distributions. This together with the seven cross sections gives a total of 139 data points. To obtain the degrees of freedom, one has to subtract from this total seven (because the program normalizes to the number of events in each angular distribution) and also the number of parameters to be varied. Typically the number of degrees of freedom was 105 to 110.

On examining the A coefficients (Fig. 5) we note that the highest order necessary to fit the data is $A6$. We take the usual approach and assume that this means that there are no significant amplitudes present higher than $G7$. The dangers of this approach are commented on later.

Since the main purpose of the experiment was to measure the branching fraction of $F7$ [$\Delta^{++}(1950)$] resonance into the $\Sigma^+ K^+$ channel, we wanted to establish that the $F7$ amplitude was (a) present and (b) resonant. To do this we started with many combinations of $S1$, $P1$, $P3$, $D3$, $D5$, $F5$, and $G7$ amplitudes but with no $F7$ present, and were unable to get a fit with a confidence level of greater than 10^{-2} . When an energy-dependent $F7$ background amplitude was substituted

TABLE III. Characteristics of various fits to the data. B denotes a background partial wave of the form $(A+Bk)e^{i(C+Dk)}$, B^* denotes a background partial wave of the form $(A+Bk)e^{iC}$, R denotes a resonant partial wave, Ampl. is defined as $(\Gamma_0/\Gamma_r)^{1/2}$, and Width is full width (Γ).

	Fit number									
	217A	192A	194A	211A	219A	218A	215A	209A	221A	200C
$S1$	B	B	B	B	B	B	B	B^*	B	B
$P1$	B	B	B	B	B	B	B	B	B	B
$P3$	B	B	B	B	B	R	B	B	B	B
$D3$	B	B	B	B	R	B	B	B	B	B
$D5$	B	B	B	R	B	B	R	B	B	B
$F5$	B	B	R	B	B	B	R	B	B	B
$F7$	B	R	R	R	R	R	R	R	R	R
$G7$	B	...
Degrees of freedom	104	105	105	105	105	105	105	106	101	148
χ^2	138	129	129	120	125	130	118	133	125	180
Confidence level	0.012	0.051	0.050	0.15	0.089	0.050	0.18	0.038	0.052	0.037
Resonance parameters										
Part. wave							$D5$			
Ampl.							0.06			
Mass (MeV)							1917			
Width (MeV)							32			
Resonance parameters										
Part. wave			$F5$	$D5$	$D3$	$P3$	$F5$			
Ampl.			0.03	0.06	0.04	0.13	0.04			
Mass (MeV)			2058	1917	1900	2386	2055			
Width (MeV)			144	32	40	1354	110			
Resonance parameters										
Part. wave		$F7$	$F7$	$F7$	$F7$	$F7$	$F7$	$F7$	$F7$	$F7$
Ampl.		0.092	0.083	0.088	0.092	0.087	0.086	0.094	0.090	0.099
Mass (MeV)		1931	1918	1973	1967	1931	1974	1965	1929	1904
Width (MeV)		294	314	266	244	356	264	250	292	284
Comments			a	b	c	d	b	e	f	g

* $F5$ amplitude small.

^b Width of $D5$ small compared with energy separation of data points.

^c Width of $D3$ small compared with energy separation of data points.

^d Mass of $P3$ outside energy range of data.

^e Energy dependence of phase of $S1$ held at zero.

^f $G7$ amplitude small.

^g Includes Purdue data at 1110, 1206, and 1265 MeV/ c (Ref. 14).

for the $G7$ amplitude, the confidence level increased to 0.014. When the $F7$ amplitude was made to be of the Breit-Wigner form, the confidence level rose to ≈ 0.05 . Table III gives a brief summary of the more probable fits (confidence level > 0.01) from the more than 200 trials. Figure 7 shows the Argand diagrams for these. By examining Fig. 7(a) it can be seen that the $F7$ amplitude is large and is looped in the right direction for a resonance even when treated as a background. By parametrizing this as a resonance [Fig. 7(b)], the confidence level is increased. The fact that the $F5$, $D5$, and $D3$ amplitudes are small makes it rather unlikely that there should be a large "background" $F7$ amplitude.

We therefore have established the presence, and probable resonant character, of the $F7$ amplitude. We then set out to establish the parameters of this amplitude and in particular to find its magnitude.

An examination of Table III shows that although the mass and width of the $\Delta(1950)$ seem to vary somewhat, the amplitude is remarkably constant and seems to depend very little on the exact nature of the higher-order background amplitudes ($D3$, $D5$, $F5$, and $G7$). This characteristic would appear to be general, and applies to all solutions which have a reasonable con-

fidence level. The Wigner condition was not used as a constraint on the energy-dependent behavior on the background amplitudes. It can be seen, for example, that in fits 192A and 194A the $S1$ amplitude is moving quite rapidly in the clockwise direction; this would appear to violate the Wigner condition. In fit 209A the energy-dependent part of the phase of $S1$ was held at zero (parameter D), and a good fit was obtained which clearly does not violate the Wigner condition. The characteristics of the $F7$ resonance are little changed; the general features of the other background amplitudes are also little changed. In any fit that has a probability of $> 10^{-2}$, we have observed the following general characteristics: a large $F7$ amplitude moving from the first to the second quadrants, consistent in behavior with a resonance; a large $S1$ amplitude in the first quadrant, decreasing somewhat with energy; a slowly varying rather small $P1$ amplitude also in the first quadrant; and a large $P3$ amplitude in the third quadrant. The presence of $D3$, $D5$, and $F5$ amplitudes increases the probability of the fit from about 1% to 18%, but all these amplitudes are small and do little to change the general features of the larger amplitudes. When the $G7$ background amplitude was added, the

best fits make it very small, consistent with zero [see, for example, fit 221A, Fig. 7(i)].

We obtain the following parameters from this analysis [assuming $\Gamma_e=0.40$ and $\Gamma_{\text{tot}}=210$ MeV, Ref. 9]:

Mass of $F7$ resonance (E_R)	1950 ± 30 MeV
Width (Γ_{tot})	300 ± 60 MeV
Amplitude ($\Gamma_e \Gamma_r$) ^{1/2}	0.090 ± 0.007
Branching ratio ($\Gamma/\Gamma_{\text{tot}}$)	$(2.0 \pm 0.4)\%$

[The values from Ref. 9 of the mass and width for the $\Delta(1950)$ are 1940 MeV and 210 MeV, respectively.] The errors quoted are estimated from the variation of values of these parameters in the various fits.

By examining Table III it can be seen that the fit can sometimes be improved by making some of the lower partial waves resonant rather than of the background form. For the $P3$ resonant amplitude, the mass is far from the experimental region, and clearly the energy dependence of the amplitude is being approxi-

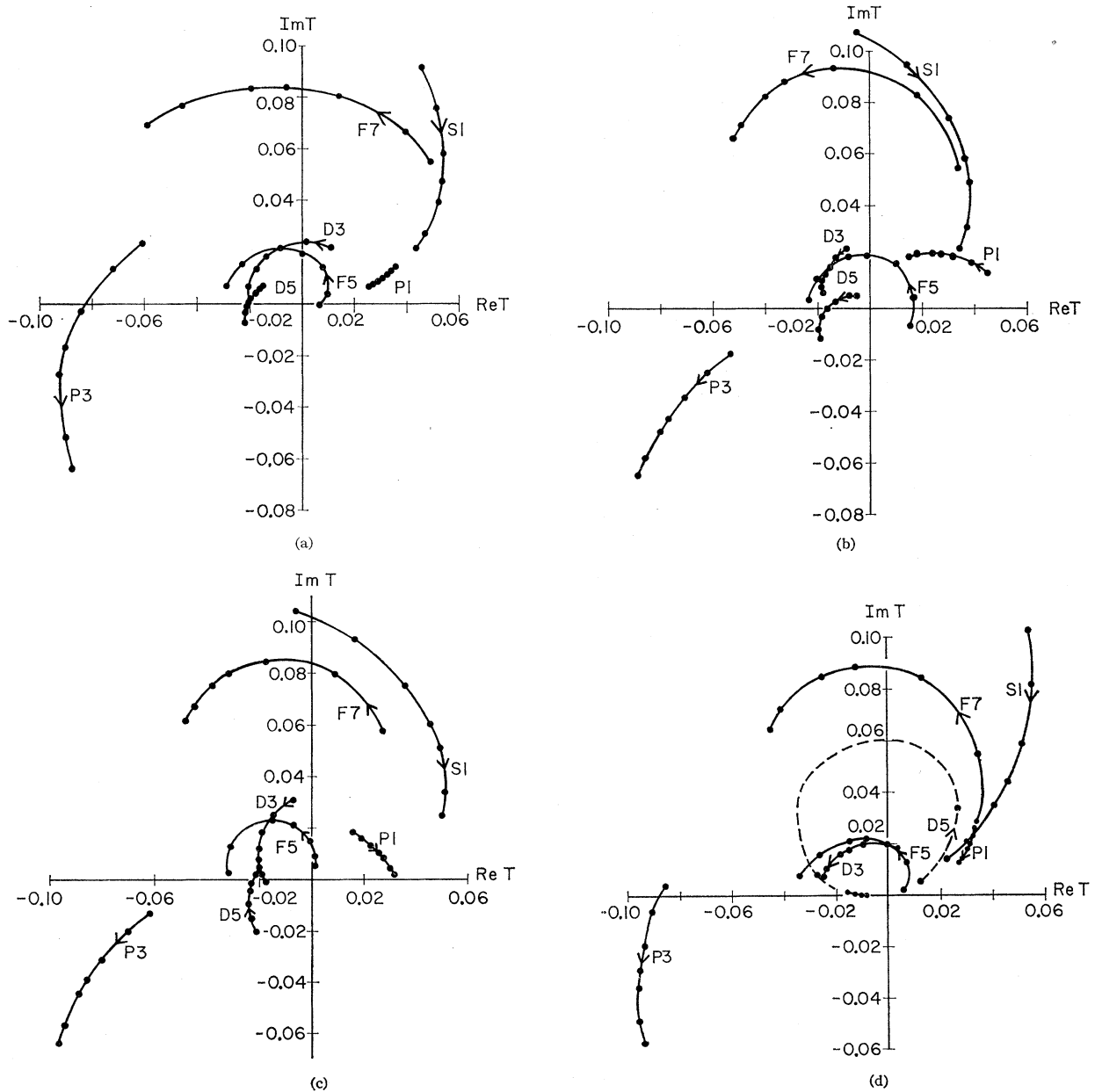


FIG. 7. Argand diagrams for the nine fits to our data summarized in Table III (s -channel approach). The phase of the resonant $F7$ amplitude in fits (b)-(i) has been taken to be zero at the resonant energy. (a) Argand diagram for fit 217A to our data (Table III); (b) for fit 192A; (c) for fit 194A; (d) for fit 211A; (e) for fit 219A; (f) for fit 218A; (g) for fit 215A; (h) for fit 209A; (i) for fit 221A.

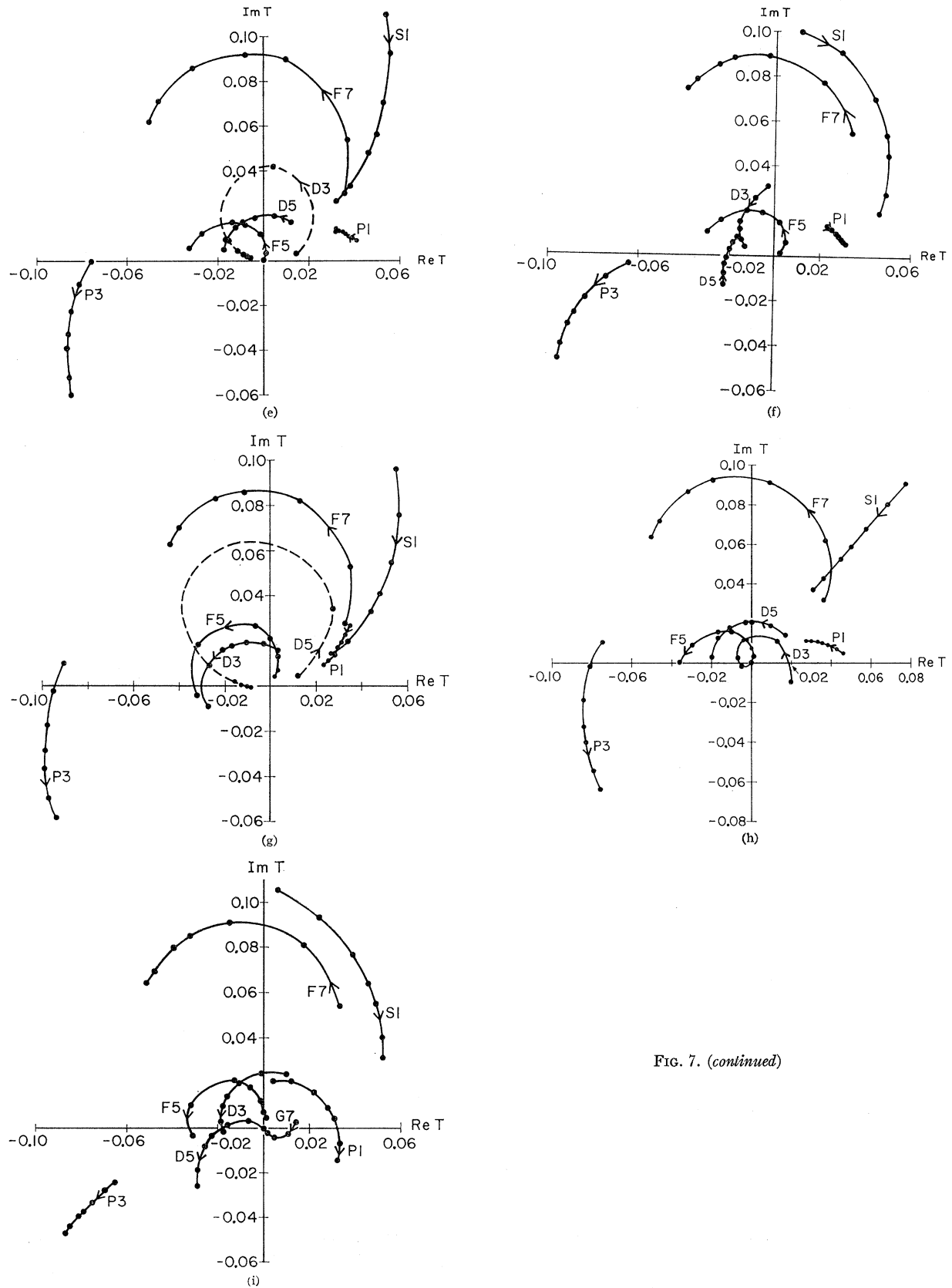


FIG. 7. (continued)

TABLE IV. Exchange-amplitude parameters.

	Evans and Knight (Ref. 1)	Dagan (Ref. 20)	Holladay* (Ref. 2)	This analysis			
				Fit 11A	Fit 14A	Fit 16A	Fit 18A
$g_{K^*K\pi}G_V$	-0.722	-0.81	-0.79	-2.7	-3.8	-3.0	-9.8
$g_{K^*K\pi}G_T$	0	0	0	-6.4	-30.3	-7.4	-36.4
ϕ_l (rad)	0	0	0.8	0.74	0.63	0.72	0.77
$g_{\pi\Lambda\Sigma}g_{N\Lambda K}$	10.8	-9.73	-13.8	-23.4	-339.0	-24.8	-19.6
ϕ_u (rad)				0.8	1.0	0.8	0.9
α				53.9	1.1	100	1.1
β				110	1.3	100	67.2

* The entries for $g_{K^*K\pi}G_V$ and $g_{\pi\Lambda\Sigma}g_{N\Lambda K}$ are found by multiplying Holladay's $G'=0.063$ and $G=0.779$ by -4π and $-4\pi\sqrt{2}$, respectively.

ated by the tail of the resonance. In the $D3$ and $D5$ amplitudes, the fitted widths are narrower than the spacing between experimental points, so that some of the experimental points lie on the tail on the low side and others on the high side. This somewhat erratic behavior (of these rather small amplitudes) increases the confidence level of the fits. The reason for this type of behavior, if real, is not clear, but cannot be well approximated by our usual background parametrization. Only for the resonant $F5$ amplitude are the mass and width reasonable.

Should the $F5$ amplitude be resonant in character, we are able to put the following upper limit on its magnitude:

$$(\Gamma_e \Gamma_r)^{1/2} < 0.04.$$

It should be emphasized that we do not believe that the data require the presence of any but the $F7$ resonance.

Since our lowest energy (1850 MeV) is not very close to threshold, we decided to check that our partial-wave analysis solutions were consistent with published lower-energy data and, in particular, we used the data of the Purdue group¹⁹ at 1730, 1783, and 1813 MeV. They had performed a single-energy fit at each of their energies. At 1730 MeV only a second-order fit in $\cos\theta$ (or a second-order term in the Legendre polynomials) was necessary, and they assumed only S and P waves were present. At the two higher energies a fourth-order term in the Legendre expansion was needed, and they therefore included S , P , and D waves in their analysis. When we compared their solutions with ours we found that they were not qualitatively similar to an extrapolation of our amplitudes. We therefore incorporated their data with ours and despite the very large energy range covered, fitted it with our usual parametrization. The fit we obtained, 200C, using as starting values the partial-wave amplitudes of solution 192A, is shown in Fig. 8 and in Table III. The solution has an over-all confidence level of 3.7% and, as can be seen, is very similar to our solution 192A. (The fit to the three Purdue energies is extremely good.) The point to note is that despite the lack of significant A coefficients (Sec. IV A) higher than A_4 at any of the Purdue energies, the

$F7$ amplitude is large, and in fact dominates at the two higher energies. This large "unsuspected" $F7$ amplitude naturally greatly modified the S , P , and D amplitudes. The contribution of this $F7$ amplitude to the sixth-order term is small enough to be covered by the experimental error.

B. s -, t -, and u -Channel Analysis

The data were handled in the way described in Sec. VI A. In this analysis, typically 14–18 varying parameters were required to produce reasonable fits. The exchange-amplitude parameters for the best solutions are given in Table IV,²⁰ along with previous determinations using similar, but not identical, approaches. (It should be noted that the parameters $g_{K^*K\pi}G_V$, $g_{K^*K\pi}G_T$, α , and β are insensitive to the data and are therefore not well determined.) The resonant-amplitude parameters for the best solutions are given in Table V.

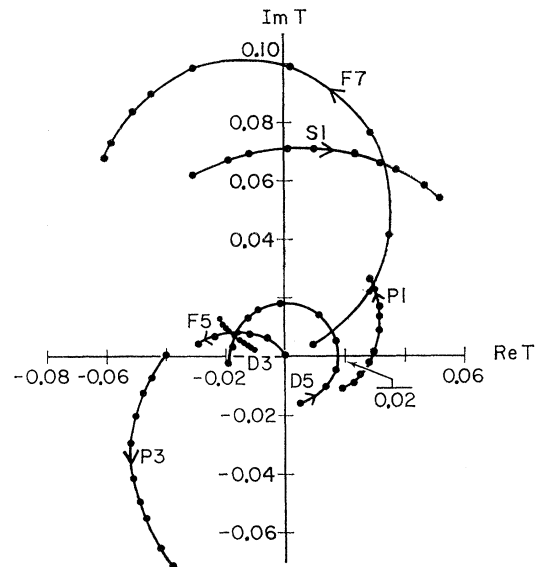


FIG. 8. Argand diagram for a fit to the data at our seven momenta and three lower momenta from the Purdue group (Ref. 19). The initial conditions for the fit were the same as fit 192A. The fitted parameters are summarized in Table III, fit 200C. The confidence level for the fit is 0.037.

¹⁹ N. L. Carayannopoulos, G. W. Tautfest, and R. B. Willmann, Phys. Rev. **138**, B433 (1965).

²⁰ S. Dagan, Z. Ming Ma, J. W. Chapman, L. R. Fortney, and E. C. Fowler, Phys. Rev. **161**, 1384 (1967).

TABLE V. Resonance parameters obtained from s -, t -, and u -channel analysis.

Fit No.	Degrees of freedom	Confidence level	Resonances								
			$(\Gamma_s \Gamma_r)^{1/2}$	$D5$ E_R	$\Gamma/2$	$(\Gamma_s \Gamma_r)^{1/2}$	$F5$ E_R	$\Gamma/2$	$(\Gamma_s \Gamma_r)^{1/2}$	$F7$ E_R	$\Gamma/2$
11A	117	0.00036	0.050	1879	40				0.99	1932	147
14A	117	10^{-6}				0.055	2128	53	0.102	1905	150
16A	113	0.028	0.057	1886	45	0.029	2071	67	0.091	1917	130
18A	113	0.035	0.056	1883	46	0.033	2099	98	0.093	1912	132

These require an $F5$ or $D5$ resonant partial wave (or both) along with the resonant $F7$. The amplitudes of these lower partial waves are smaller than the $F7$ amplitude and provide some necessary total angular momentum $J = \frac{5}{2}$ amplitudes which cannot be supplied by the exchange terms. Figure 9 shows the Argand plot for two of these fits, where the t - and u -channel contributions to the amplitude have been projected into the s channel in the manner described in Sec. IV B, and the other parameters of the $\Delta(1950)$ are quite consistent with those given in Sec. V A. In comparing these parameters with those from the s -channel partial-wave analysis, we see that the $F7$ amplitudes are virtually identical. This is further evidence that the precise nature of the other partial waves in the reaction seems not to affect the magnitude of the principal $F7$ partial wave.

The seriousness of double counting was studied by not using any resonant amplitudes and trying to fit the data with only exchange amplitudes. No satisfactory fit was achieved, nor were there any significant contributions to the $l \geq 3$ partial waves from the exchange terms. We therefore believe that double counting is not likely to be serious in this case.

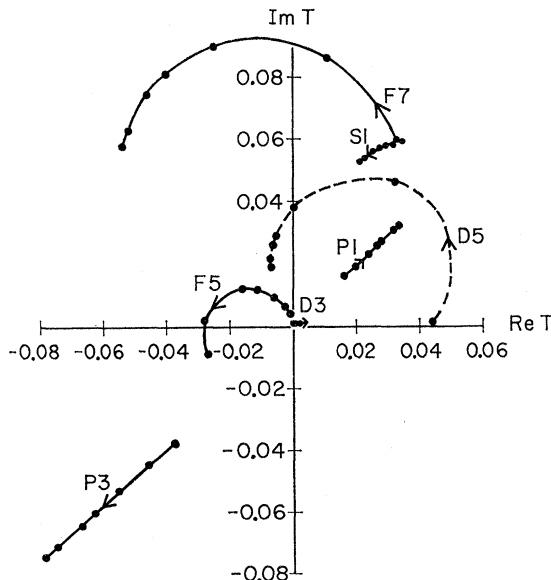


FIG. 9. Argand diagram for a fit to our data using the s -, t -, and u -channel approach, where the t - and u -channel amplitudes have been projected into the s channel. The parameters of the fit are given in Tables IV and V.

It should be noted that although there are serious theoretical objections to this model as it stands, for the purpose of determining the branching fraction of the $\Delta(1950)$ into the $\Sigma^+ K^+$ channel these are not very relevant. The t - and u -channel exchange formalism provides a parametrization of the "background" amplitudes that is different from that used in the s -channel approach. Good fits have been obtained by using a significantly smaller number of parameters than for the s channel.

In comparing the two analyses for the "background" contributions to the amplitude, several points should be made.

(i) In principle, in the exchange model, all partial waves are present and are parametrized by seven variables. [In practice, only the first four partial waves ($S1$, $P1$, $P3$, and $D3$) can be present in appreciable quantities.] In the s -channel analysis, four parameters per partial wave are required.

(ii) The s -channel approach does not have the objection of double counting which the other analysis does have in principle—although not in practice.

(iii) In the exchange model, the parametrization is such that the $P1$ and higher partial-wave amplitudes (when the exchange amplitude has been projected into the s channel) increase monotonically with energy, eventually violating unitarity. This consideration is not important in our energy region. This problem is not encountered in the s -channel analysis.

VII. DISCUSSION

Using both of our approaches, we have found sets of partial waves which adequately fit all our data. These fits, as can be seen from Tables III and V and Figs. 7 and 9, are very similar in general features and, in particular, give consistent values for the parameters of the $\Delta(1950)$. We do not believe that we can establish the character of the $D3$, $D5$, and $F5$ amplitudes; they could be either of a resonant or of a background nature. However, they appear to be small and not important in obtaining the parameters of the $\Delta(1950)$. It should be noted that other solutions that give identical fits can be manufactured by applying the Minami and Yang transformation to our solutions. This will have the effect of increasing the number of resonances. It should also be pointed out that our not finding any other solution that is radically different from the ones pre-

sented must be interpreted within the framework of the models and assumptions used. In particular, the dangers of neglecting the presence of higher partial waves than appear to be necessary is clearly illustrated in the case of the Purdue low-energy data. This problem is common not just to these results but to virtually all partial-wave analysis results published.

Finally, we make a comparison of the branching fraction, $(2.0 \pm 0.4)\%$, obtained for $\Delta(1950) \rightarrow \Sigma^+ K^+$ with the $SU(3)$ prediction.

Assuming that the $\Delta(1950)$ is in a decuplet, one can write the partial widths as²¹

$$\Gamma_i = c_i^2 g^2 B_l(p_i) (M_N/M_R) p_i,$$

where c is the $SU(3)$ Clebsch-Gordan coefficient for each decay mode, g is the effective coupling constant [and is the same for every decay mode if $SU(3)$ is not broken], $B_l(p)$ is the centrifugal-barrier factor for an angular momentum l , p is the c.m. decay momentum, M_R is the resonant mass, and M_N is the nucleon mass.

$\Gamma[\Delta(1950) \rightarrow \pi p]$ is well established from phase-shift analyses [we use $\Gamma_{\pi p}/\Gamma_{\text{tot}} = 0.4$],⁹ so that

$$\Gamma_{\Sigma K}/\Gamma_{\pi p} = B_l(p_{\Sigma K}) p_{\Sigma K} / [B_l(p_{\pi p}) p_{\pi p}],$$

since $g_{\Sigma K} = g_{\pi p}$ and $c_{\Sigma K} = c_{\pi p}$; the form of $B_l(p)$ is given in Blatt and Weisskopf.¹² For $l=3$,

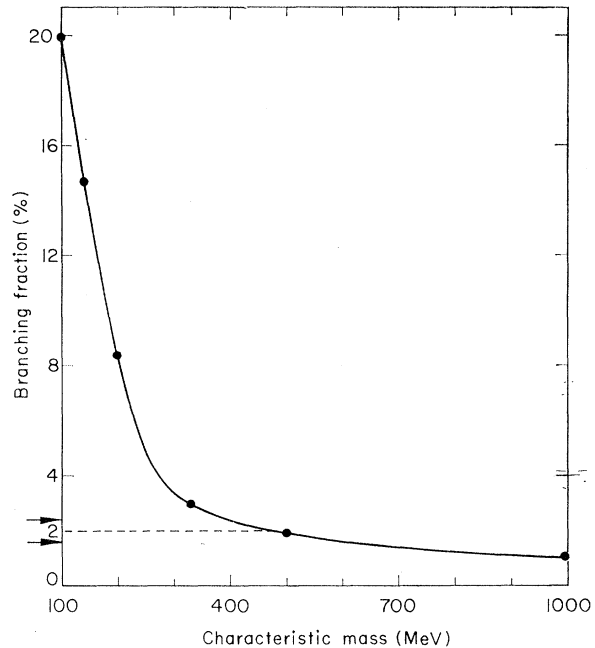
$$B_l(p) = (pr)^6 / [225 + 45(pr)^2 + 6(pr)^4 + (pr)^6],$$

where r is the radius of interaction.

Figure 10 shows a plot of $\Gamma_{\Sigma K}/\Gamma_{\text{tot}}$ as a function of $1/r$ (GeV). The value of $1/r$ associated with our measurement of $\Gamma_{\Sigma K}/\Gamma_{\text{tot}}$ is 475 MeV, with the errors shown on the figure. This measurement of $1/r$ is very sensitive because of the large difference between $p_{\Sigma K}$ and $p_{\pi p}$. This may be compared with the value appropriate to the $\frac{3}{2}^+$ decuplet $\Delta(1236)$, which is ≈ 160 MeV.²² [This value is found by detailed fitting of the

²¹ R. D. Tripp, in *Proceedings of the Fourteenth International Conference on High-Energy Physics, Vienna, 1968* (CERN, Geneva, 1968), p. 185.

²² M. Gell-Mann and K. M. Watson, *Ann. Rev. Nucl. Sci.* 4, 231 (1954).



XBL703-2621

FIG. 10. Plot of $\Gamma_{\Sigma K}/\Gamma_{\text{tot}}$ as a function of $1/r$ (MeV).

shape of the $\Delta(1236)$, and therefore has been obtained by a method different from ours.] The $SU(3)$ prediction of branching ratio of the $\Delta(1950) \rightarrow \Sigma^+ K^+$ deduced from this value of $1/r$ is 13%, which is not in agreement with our measured value.

ACKNOWLEDGMENTS

We thank Dr. Robert Tripp, Dr. Robert Ely, and Dr. Robert Birge for helpful discussions. We are indebted to Dennis Hall, Vivian Morgan, and Loren Shultz of the Data Handling Group, and to the scanners and measurers of the Powell-Birge Group, whose efforts at finding and measuring the rare and elusive Σ 's were the basis of this experiment.